



Assessing the tropical Atlantic biogeochemical processes in the Norwegian Earth System Models

Shunya Koseki¹, Lander R. Crespo¹, Jerry Tjiputra², Filippa Fransner¹, Noel S. Keenlyside^{1,3} David Rivas^{1,4}

5 ¹Geophysical Institute, University of Bergen / Bjerknes Centre for Climate Research, Bergen, 5007, Norway

²NORCE Norwegian Research Centre / Bjerknes Centre for Climate Research, Bergen, 5838, Norway

³Nansen Environment and Remote Sensing Centre/ Bjerknes Centre for Climate Research, Bergen, 5007, Norway

⁴Centro de Investigación Científico y de Educación Superior de Ensenada, Ensenada, 22860, Mexico

10 *Correspondence to:* Shunya Koseki (Shunya.Koseki@uib.no)

Abstract. State-of-the-art Earth system models exhibit large biases in their representation of the tropical Atlantic hydrography, with potential large impacts on both climate and ocean biogeochemistry projections. This study investigates how biases in model physics influences marine biogeochemical processes in the tropical Atlantic using the Norwegian Earth System Model (NorESM). We assess four different configurations of NorESM: NorESM1 is taken as benchmark
15 (NorESM1-CTL) that we compare against the simulations with (1) a physical bias correction and against (2 and 3) two configurations of the latest version of NorESM with improved physical and biogeochemical parameterizations with low and intermediate atmospheric resolutions, respectively. With respect to NorESM1-CTL, the annual-mean sea surface temperature (SST) bias is reduced largely in the first and comparably third simulations in the equatorial and southeast Atlantic. In addition, the SST seasonal cycle is improved in all three simulations, resulting in more realistic development of the Atlantic
20 Cold Tongue in terms of location and timing. Corresponding to the cold tongue seasonal cycle, the marine primary production in the equatorial Atlantic is also improved and in particular, the Atlantic summer bloom is well represented during June to September in all three simulations. The more realistic summer bloom can be related to the well-represented shallow thermocline and associated nitrate supply from the subsurface ocean at the equator. The climatological intense outgassing of sea-air CO₂ flux in the western basin is also improved in all three simulations. Improvements in the
25 climatology mean state also lead to better representation of primary production and sea-air CO₂ interannual variability associated with the Atlantic Niño and Niña events. We stress that physical process and its improvement are responsible for modeling the marine biogeochemical process as the first simulations, where only climatological surface ocean dynamics are corrected, provides the better improvements of marine biogeochemical processes.



30 1 Introduction

The tropical Atlantic Ocean is a region with intense biogeochemical cycling and productive ecosystems resulting in a hotspot for large fisheries (Gregg et al., 2003; Menard et al., 2000). In particular, the characteristics of the marine ecosystems in the tropical Atlantic are manifested by the high marine biological production along the west African coast associated with the Canary and the Benguela upwelling systems (Hutchings et al., 2009; Santos et al., 2007; Shannon et al., 35 2004; Vazquez et al., 2022). Another key driver of the marine ecosystem in the tropical Atlantic is riverine flux from the great rivers like the Congo and Amazon Rivers (Araujo et al., 2014; Bouillon et al., 2012; Demaster and Pope, 1996; Moreira-Turcq et al., 2003; Vieira et al., 2020). The coastal upwelling and riverine fluxes are important sources of nutrients such as nitrate (NO_3^-), phosphate (PO_4^{3-}), and silicate (SiO_2) for phytoplankton (Gao et al., 2023). Apart from the coastal areas, high marine production is also observed in the central to eastern basin of the equatorial Atlantic where the Atlantic Cold Tongue (ACT, Crespo et al., 2019; Hummels et al., 2013; Okumura and Xie, 2006; Tokinaga and Xie, 2011), 40 associated with cold sea surface temperature (SST), develops during boreal summer (June-July-August). Here, a seasonal high production is fueled by the equatorial upwelling that supplies nutrient-rich seawater from the subsurface ocean (Chenillat et al., 2021; Kawase and Sarmiento, 1985; Perez et al., 2005). In addition to this predominant seasonal variation, the primary production in the equatorial Atlantic has a strong inter-annual variability associated with the Atlantic Niño and 45 Niña (Crespo et al., 2022; Keenlyside and Latif, 2007; Prigent et al., 2020) that has its peak during boreal summer (Chenillat et al., 2021). The Atlantic Niño and Niña are, in general, induced by modifications in the equatorial upwelling and thermocline zonal gradient via the Bjerknes Feedback (Bjerknes, 1969; Crespo et al., 2022; Keenlyside and Latif, 2007; Prigent et al., 2020) while other possible mechanisms are also discussed such as thermodynamical driver and warm water advection from subtropical (Nnamchi et al., 2021; Nnamchi et al., 2015; Richter et al., 2013). Chenillat et al. (2021) showed 50 that the upwelling changes associated with such Atlantic dynamical variability mode is predominantly responsible for the interannual variability in the equatorial Atlantic summer high production.

In addition to the high productivity, the tropical Atlantic Ocean plays an important role in the global carbon cycle (Takahashi et al., 2002). Model projections indicate that the tropical Atlantic is a key convergence zone for anthropogenic carbon in the future (Tjiputra et al., 2010), with rapid and long-term climate change imprints, such as warming, ocean 55 acidification, and oxygen changes in the future (Bertini and Tjiputra, 2022; Tjiputra, 2023). The sea-air carbon dioxide (CO_2) flux in the tropical Atlantic Ocean is predominantly outgassing, making it the second largest CO_2 outgassing system in the global ocean (Sarmiento, 2006). This large CO_2 outgassing is mainly attributed to rich dissolved inorganic carbon that is supplied from subsurface ocean by the equatorial upwelling (Koseki et al., 2023) and enhances the surface partial pressure of CO_2 ($p\text{CO}_2$). In addition to dissolved inorganic carbon, $p\text{CO}_2$ is a function of several oceanic physical-chemical properties 60 like SST, sea surface salinity (SSS), and total alkalinity (Sarmiento and Gruber, 2006). Lefevre et al. (2013) suggested that SST and SSS positive anomalies in the northern tropical Atlantic enhance the outgassing of CO_2 flux during February to

May. More recently, Koseki et al. (2023) showed a unique pattern and mechanism of CO₂ flux anomalies associated with the Atlantic Niño and Niña, which is distinct from that in the tropical Pacific (Ayar et al., 2022).

65 With the rapid development of computational technologies and resources, marine biogeochemical models are now standard components of Earth system models (ESMs), which have become key tools to investigate the global carbon cycle, marine physical-biogeochemical interaction and their feedbacks on the global and regional climate (Doney, 1999; Ilyina et al., 2013; Kriest and Oschlies, 2015; Seferian et al., 2020; Sein et al., 2015). They are also widely used to produce near-term predictions of the interannual to decadal evolution of the marine biogeochemistry (Fransner et al., 2020; Seferian et al., 2018; Seferian et al., 2019). These prediction models have added important evidence that ocean physics plays a major role in
70 shaping marine biogeochemical processes. For example, Ramirez-Romero et al. (2020), using four different coupled physical-biogeochemical model configurations, suggested that the intensity, timing and vertical location of deep chlorophyll maximum are very sensitive to the ocean stratification period and intensity. Fransner et al. (2020) showed that physical processes play a crucial role in controlling the nutrients and primary production variability and consequently the predictability of key biogeochemical processes such as CO₂ fluxes. It had been demonstrated that biases in physical
75 dynamics can bring about large uncertainty in future projections of ocean carbon sink (Bourgeois et al., 2022; Goris et al., 2023; Goris et al., 2018). Therefore, to improve the fidelity of future projections of ocean carbon cycle at regional scales, it is very important to understand the physical-biogeochemical interactions and verify how properly such interaction is simulated by the ESMs.

As a long-standing common issue, most of the advanced ESMs exhibit non-negligible systematic physical biases in
80 the representation of climate variables in the tropical Atlantic such as SST, precipitation, and other relevant atmospheric and oceanic fields (de la Vara et al., 2020; Koseki et al., 2018; Mohino et al., 2019; Voltaire et al., 2019), which can degrade predictability of climate variability (Counillon et al., 2021). The origins of such systematic biases are diverse among the ESMs: imperfect parameterization of ocean mixed layer processes (Deppenmeier et al., 2020), coarse resolution of atmospheric and oceanic components (de la Vara et al., 2020; Harlass et al., 2018), intrinsic atmospheric bias of surface wind
85 (Koseki et al., 2018; Xu et al., 2014) and poor representation of subtropical atmospheric surface circulation (Cabos et al., 2017). The tropical Atlantic SST biases also exacerbate the climate variability and predictability (e.g., Counillon et al., 2021; Dippe et al., 2018; Prodhomme et al., 2019). While these physical and dynamical biases of the ESMs have been widely discussed during this decade, there are limited studies on their impact on the simulated marine biogeochemical processes in the tropical Atlantic.

90 Here, we assess the impact of physical and dynamical biases on the representation of biogeochemistry in the tropical Atlantic in one CMIP (Coupled Model Intercomparison Project) -class ESM, the Norwegian Earth System Model (NorESM). We evaluate three simulations with (1) physical bias correction, (2) better parameterizations of atmosphere/ocean physical and marine biogeochemical processes, and (3) refinement of atmospheric model spatial resolution. Focusing on physical properties like SST and the thermocline, we investigate to what extent the biogeochemical
95 processes are improved in terms of climatology, seasonality, and inter-annual variability. This paper is structured as follows.



Section 2 gives the details of NorESM, its experimental settings, and the observational data used for verification. In Section 3, we show and discuss the results of NorESM simulations. Finally, this paper is summarized in Section 4.

2 Norwegian Earth System Model and Data

2.1 Model description

100 The first generation Norwegian Earth System Model (NorESM1, Bentsen et al., 2013), which contributes to the phase 5 of CMIP exercise (Taylor et al., 2012), consists of the Community Atmospheric Model version 4 (CAM4, Neale, 2010), the Miami Isopycnic Coordinate Model (MICOM; (Bleck et al., 1992), the Community Sea Ice Model (CICE4), the Community Land Surface Model (CLM4) and the Hamburg Ocean Carbon Cycle model (HAMOCC, Tjiputra et al., 2013). NorESM2 is the latest generation of NorESM with updates and tunings of physical and biogeochemical parameterization
105 ((Seland et al., 2020; Tjiputra et al., 2020) and contributor to CMIP6 (Eyring et al., 2016). The atmospheric component is updated to CAM6-Nor with axial angular momentum conservation (Toniazzi et al., 2020) and parameterization for atmosphere-aerosol-radiation is employed. The ocean component of NorESM2 is replaced with the Bergen Layered Ocean Model (BLOM) that implements the updated parameterization of second-order closure scheme (Ilicak et al., 2008). HAMOCC is updated to iHAMOCC (Tjiputra et al., 2020). More details of NorESM2 description and broad scale evaluation
110 of its physics and ocean biogeochemistry are available in (Seland et al., 2020; Tjiputra et al., 2020).

2.2 Model configurations

With NorESM1 we performed a standard historical simulation. As a benchmark simulation, referred to as NorESM1-CTL, NorESM1 was initialized at 1980-01-15 from a historical spin-up starting at 1850-01-01 following
115 (Counillon et al., 2021). The initial conditions of HAMOCC we obtained from a historical run of (Tjiputra et al., 2013). NorESM1-CTL was integrated until the end of 2019. In the second model configuration, an anomaly coupling technique (Toniazzi and Koseki, 2018) was implemented into NorESM1 to reduce physical biases. In this methodology, the model's monthly climatologies of SST and surface wind were replaced by the observed ones during the model integration at every coupling step while the frequency of air-sea coupling was kept identical to NorESM1-CTL. The observed SST and surface
120 wind were obtained from HadISST and ERA-Interim (Dee et al., 2011) respectively for 1980-2000. This run is referred to as NorESM1-AC, and ocean carbon cycle is included as in NorESM1-CTL. Other details of NorESM1-CTL and NorESM1-AC (for example, spin-up duration, model performance, etc) can be found in Counillon et al. (2021). Due to the initial physical adjustments on the biogeochemistry, we considered the first 10 years of NorESM1-CTL and NorESM1-AC as adjustment period and were not analyzed in our study.

125 Two historical runs of NorESM2 (NorESM2-LM and NorESM2-MM) following the standard CMIP6 protocol were integrated from 1850 until 2014 and the data from 1990 to 2014 period are analyzed in this study. NorESM2-LM and NorESM2-MM differ in the spatial resolutions of the atmospheric model CAM6-Nor with a coarse resolution of $2.5^{\circ} \times 1.9^{\circ}$



and an intermediate resolution of $1.5^{\circ} \times 0.9^{\circ}$, respectively. The resolution of the ocean component is similar in all simulations of NorESM1 and NorESM2. On the other hand, the resolution of atmospheric components is equal for NorESM1 and
130 NorESM2-LM. The simulations of NorESM1 and NorESM2 each have 5 and 3 ensemble members, respectively. These experimental settings are given in Fig. S1. To summarize, NorESM1-AC is a reference for physical bias correction and NorESM2-LM/MM are for improved physical and biogeochemical parametrizations in comparison with the benchmark simulation of NorESM1-CTL. We also aim to qualitatively assess the impacts of model refinement on simulation performance by comparing with NorESM1-CTL with NorESM2-LM and NorESM2-MM.

135

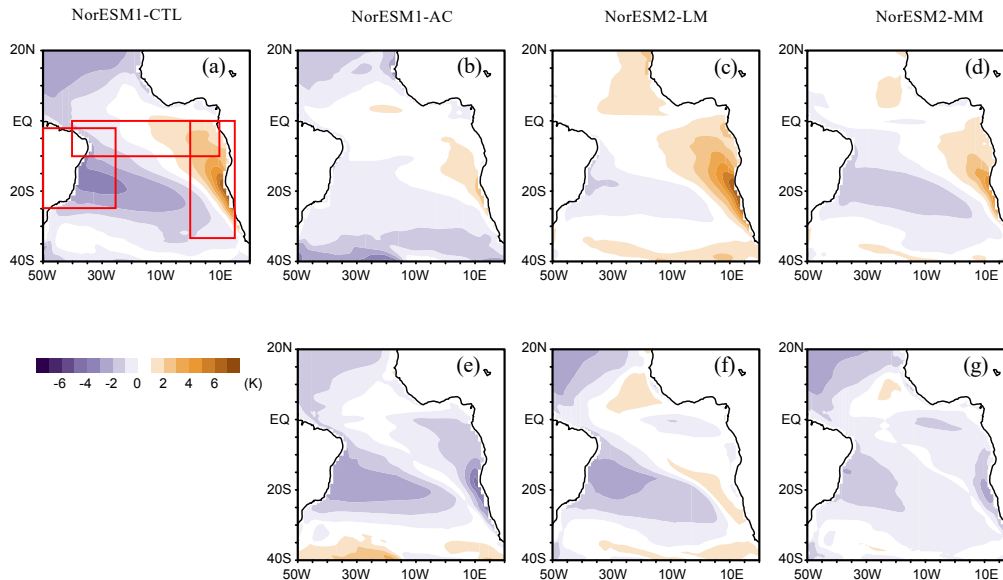
2.3 Observational data

We evaluate the NorESM simulations using observational datasets. The SST data is from Optimum Interpolated SST (OISST, Reynolds et al., 2007) from 1990 to 2019. Three dimensional ocean data of temperature, nitrate and phosphate were taken from World Ocean Atlas 18 (WOA18, Locarnini et al. 2018; Garcia et al., 2018) climatological data. Monthly
140 marine primary production was taken from MODIS (Moderate Resolution Imaging Spectroradiometer) satellite data from 2003 to 2019. The ocean surface CO₂ flux is from the global observation-based gridded data of Landschutzer et al. (2016) and Landschutzer et al. (2020) from 1990 to 2015.

3 Results

3.1 Climatology

145 First, we assess the SST bias in our four experiments (Fig. 1). NorESM1-CTL has a warm bias along the west African coast (Fig. 1a), which is a common bias in ESMs (Richter, 2015). In contrast, cold SST biases are detected in the subtropics. The causes of the SST bias in NorESM1 are predominantly erroneous wind stress and air-sea heat flux (Koseki et al., 2018). By implementing the anomaly coupling technique (NorESM1-AC), the tropical Atlantic SST biases are substantially alleviated (Fig. 1b, e). In particular, the warm bias of the Angola-Benguela Frontal Zone (ABFZ, 15°S to 17°S
150 along the western African coast, e.g., (Koseki et al., 2019) is reduced by up to 5°C. NorESM2-LM also exhibits a considerably warm bias in the eastern tropical Atlantic while the subtropical cold biases are reduced at the south and even suppressed in the north (Fig. 1c). The improvement of the subtropical Atlantic is comparable with that of NorESM1-AC (Fig. 1e and f). The summer (June-July-August) SST bias is comparably alleviated between NorESM1-AC and NorESM2-LM (Fig. S2). In NorESM2-MM, the SST bias is reduced more than NorESM2-LM (Fig. 1d). The ABFZ warm bias in
155 NorESM2-MM is improved by 3°C and the equatorial Atlantic by 2°C (Fig. 1g and Fig. S2). Comparison between NorESM2-LM and NorESM2-MM suggests that a horizontal refinement of the atmospheric model improves the climatic state of the surface ocean, consistent with (Harlass et al., 2018).



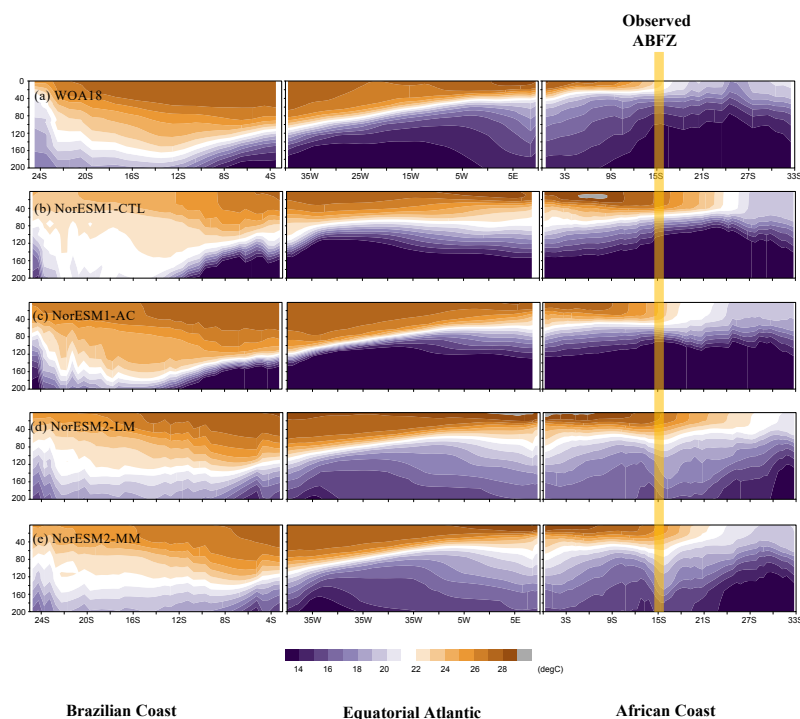
160

Figure 1: (a)-(d) Annual-mean climatological bias of sea surface temperature (SST) with respect to OISST data and (e)-(g) bias improvements of each simulation compared to NorESM1-CTL. In (e)-(h), the negative (positive) values indicate improvement (exacerbation) compared to NorESM1-CTL. The red boxes denote the area for averaging in Fig.2.

165

Figure 2 provides vertical sections of the observed and simulated ocean temperature around the south pan-tropical Atlantic Ocean. In the observation, a thick warm layer forms around the northeast Brazilian coast and western equatorial Atlantic while a thin warm layer penetrates from the eastern equatorial Atlantic to the ABFZ resulting in the east-west tilting thermocline depth along the equator (Fig. 2a). NorESM1-CTL fails to reproduce the east-west steep gradient of thermocline along the equator and the observed warm pool in the western Atlantic and northeastern Brazilian coast (Fig. 2b). The thick warm layer is homogeneously formed along this pan-tropical Atlantic sector and the ABFZ is pushed further southward. By applying the physical bias reduction (NorESM1-AC), the equatorial thermocline zonal-gradient bias is alleviated and the thick warm pool is generated more realistically than in NorESM1-CTL (Fig. 2c). The erroneous southward penetration of warm water along the African coast is suppressed, resulting in reduction of the warm SST bias in NorESM1-AC (Fig. 1b, c). While the zonal-tilting of the equatorial thermocline is well represented in NorESM2-LM, the warm pool is relatively shallower than NorESM1-AC in the western Atlantic and the ABFZ is pushed further southward comparable with NorESM1-CTL (Fig. 2d). In NorESM2-MM, the tilting thermocline is similarly well represented along the equator, and the location of the ABFZ are more realistic than NorESM2-LM. Compared to observation and NorESM1, NorESM2 tends to have warmer subsurface ocean (Fig. 2d and e).

175



180 **Figure 2:** Depth sector of annual-mean climatology of ocean temperature along Brazilian coast, equatorial Atlantic, and African coast for observation and each NorESM simulation averaged in the three boxes shown in Fig. 1a. Yellow line denotes the location of the Angola-Benguela Frontal Zone (ABFZ) in the observation.

3.2 Seasonality

185 Figure 3a-e illustrates temporal-longitude Hovmöller plots of SST in the equatorial Atlantic for observation and each model simulation. In the observations, the SST shows a clear seasonal cycle (Crespo et al., 2019; Ding et al., 2009) with the ACT developing in the boreal summer. NorESM1-CTL reproduces roughly the seasonal cycle of SST, but it fails to simulate the location and timing of the ACT: the ACT peak occurs more westward in the equator (30°W) and its peak is slightly later than in the observation (Fig. 3b). This discrepancy is consistent with the thick and zonally uniform warm layer along the entire equatorial Atlantic (Fig. 2b). Employment of the climatological bias correction leads to a more realistic development of the ACT, in particular, the location of the ACT is well represented (Fig. 3c; (Toniazzi and Koseki, 2018). Note that the anomaly coupling corrects directly the climatological surface wind forcing in the ocean model. In NorESM2 simulations, the SST seasonal cycle is also improved and NorESM2-MM has a stronger ACT with better timing during summer than NorESM2-LM (Fig. 3d and e).

195 Next, we investigate the simulation in surface biogeochemistry, which is tightly linked to physical dynamics and SST (e.g., Chenillat et al., 2021). Figure 3f-j shows the temporal-longitude Hovmöller plot of climatological primary production for observation and each simulation. In the observations, the primary production has a clear seasonal cycle with a

200 peak between 20°W and 0° in JJA ($0.075 \text{ mol C m}^{-2} \text{ day}^{-1}$), which is consistent with the spatiotemporal development of the ACT (Fig. 3a, f). There is another less pronounced high productivity season during November to January in the equatorial Atlantic (Fig. 3f). NorESM1-CTL simulates the summer bloom very poorly (Fig. 3g).

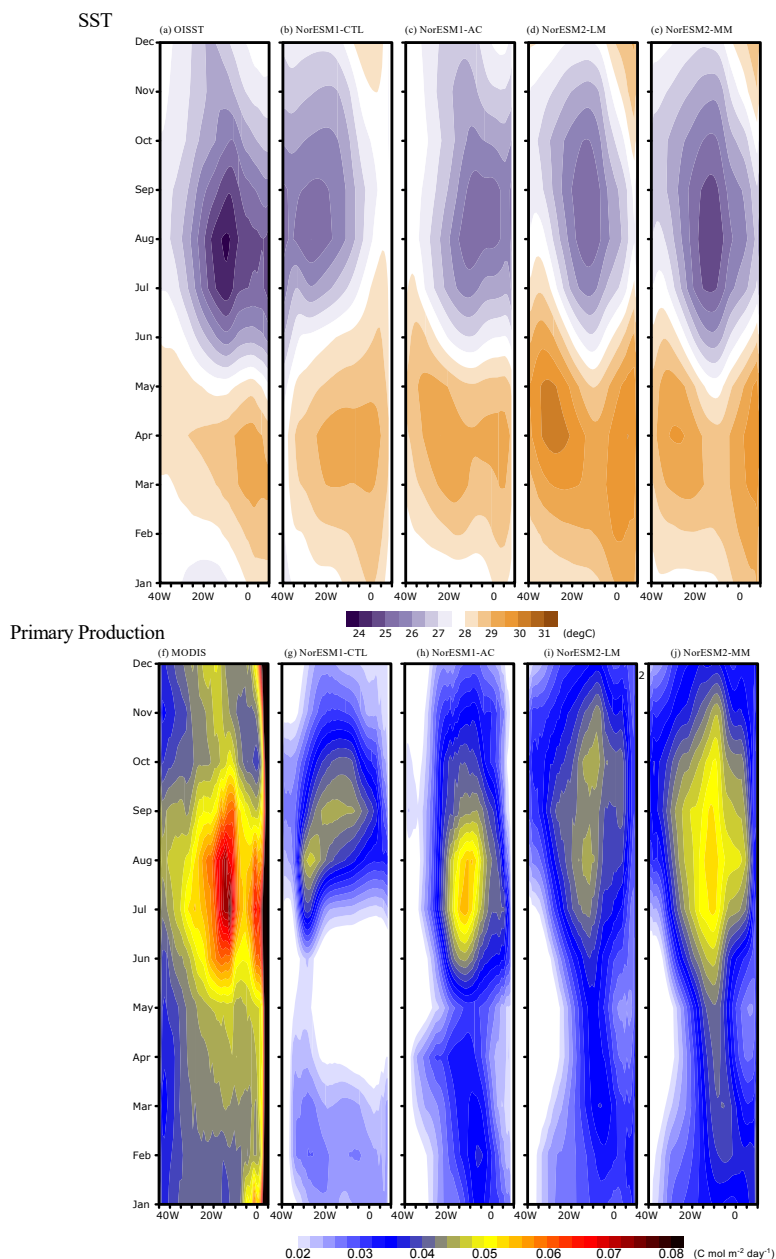
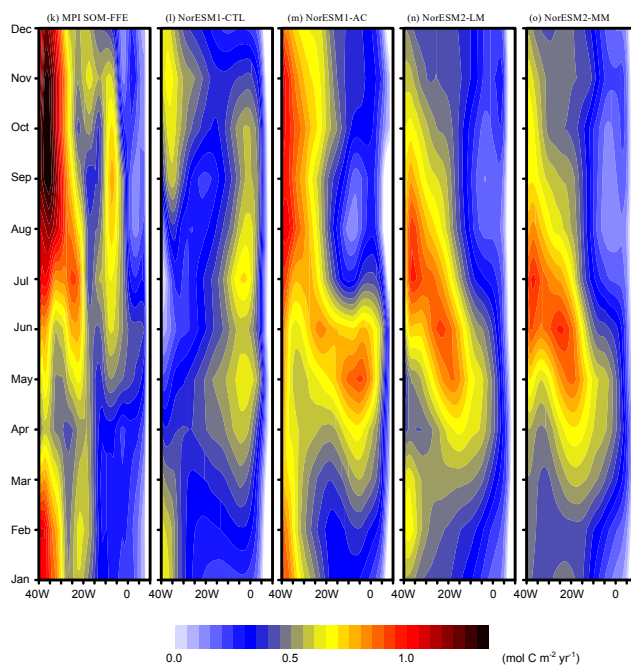


Figure 3: Climatological seasonal cycle of (upper row) SST and (lower row) primary production for observation and each simulation of NorESM along the equator (averaged 3S-3N). The observed primary production is obtained from MODIS satellite data. The modelled primary production is vertically integrated through the entire ocean layer.



205

The peak of the summer bloom is weaker, located more westward (30°W), and occurs later, in August and September, than in the observations. Apart from the summer bloom, there is another peak in February in the western basin and nearly no production in April to May. Interestingly, the climatological bias corrected simulation NorESM1-AC is able to reproduce the
210 observed timing and location of the summer bloom (Fig. 3h). The intensity of the summer bloom also increases (up to 0.055 mol C m⁻² day⁻¹) even though it is 27% lower than the observations. In the two NorESM2 simulations, the summer bloom tends to be better represented than in NorESM1-CTL (Fig. 3i and j). However, the summer bloom in NorESM2-LM is weak (approximately 0.043 mol C m⁻² day⁻¹) and there is a double-core peak in August and October. On the other hand, NorESM2-MM has a stronger summer bloom with a more realistic timing similar to NorESM1-AC. These differences in primary
215 production in the NorESM2 simulations can be attributed to the differences in the ACT development (Fig. 3d and e). All the NorESM simulations fail to reproduce the very high coastal production in the east, which will be discussed in the last paragraph of this subsection.



220 **Figure 3:** Continued. Climatological seasonal cycle of sea-air CO₂ flux. Positive value denotes upward.



The Hovmöller plot of sea-air CO₂ flux along the equator is given in Fig.3k-o. In the observations, the CO₂ flux has a clear seasonal cycle: particularly, maximum CO₂ flux outgassing during July to October in the western (40°-30°W) and eastern (10°W-0°) basins while the outgassing is modest in the central (20°W) basin (Fig. 3k). The late summer peak of the CO₂ flux in the central-eastern basin could be associated with the development of ACT that supplies the anomalously high dissolved inorganic carbon (DIC) water mass from the subsurface (Koseki et al., 2023). Contrastingly, in the western basin where such upwelling is weaker the outgassing may be related to the solubility of CO₂ gas. As Lefevre et al. (2013) and Koseki et al. (2023) suggest, the solubility of CO₂ gas (a function of temperature and salinity) is responsible for the inter-annual variability in *p*CO₂ and consequently sea-air CO₂ flux in the tropical Atlantic. In the western basin, the CO₂ outgassing is moderate in April when the precipitation is strongest (not shown) along the western equatorial Atlantic and in contrast, the timing of intense outgassing (August to October) is consistent with the period when the inter-tropical convergence zone (ITCZ) sits further northward from the equator.

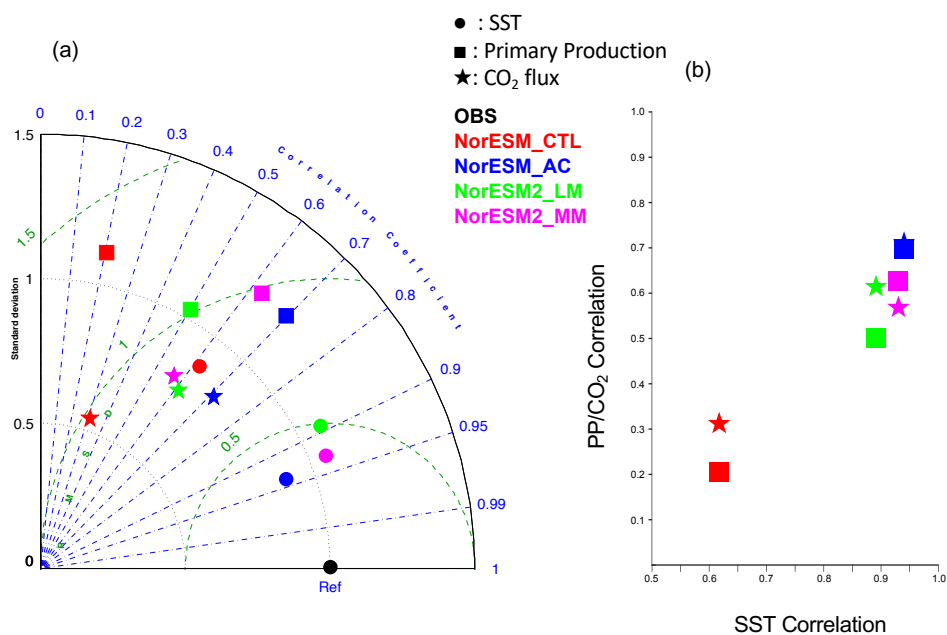
NorESM1-CTL poorly reproduces the seasonal march of CO₂ distribution (Fig. 3l): the eastern outgassing shifts more eastward and it occurs one or two months earlier. In the western basin, the observed vigorous outgassing is not simulated well, except for some weak outgassing from September to March. In NorESM1-AC, the observed outgassing in the western basin is particularly well simulated from July to November although its magnitude is relatively modest (Fig. 3m). In the central to eastern basin, the early occurrence of intense outgassing remains. Similar to the primary production, improvement in the two NorESM2 simulations (Fig. 3n and o) relative to NorESM1-CTL is also evident for CO₂ flux. Nevertheless, the timing of the seasonal cycle in the eastern basin shifts considerably.

Compared to NorESM1-CTL, all other NorESM simulations improve the SST, primary production, and sea-air CO₂ flux seasonal cycle in a statistical way (Fig. 4). In particular, NorESM1-AC performs the best, followed by NorESM2-MM in reproducing the observed seasonal variations in SST and correspondingly sea-air CO₂ flux, and primary production (Fig. 4a). The pronounced improvements in the NorESM1-AC indicates that the atmospheric circulation is crucially responsible for representation of SST, PP and CO₂ flux in the tropical Atlantic. Indeed, the SST in this region is highly influenced by the wind inducing upwelling (e.g., Voltaire et al., 2019), which also supplies nutrients to the surface ocean that fuels PP. The improvement of sea-air CO₂ flux is almost identical between NorESM2-LM and NorESM2-MM. A scatter plot between SST and biogeochemical correlations clearly shows that the better simulation of SST seasonal cycle is important for simulating the seasonal cycle of biogeochemical processes (Fig. 4b).

Because the summer bloom in the tropical Atlantic is connected closely to the availability of nutrients (e.g., Radenac et al., 2020), here we assess the subsurface nutrient concentrations during JJA (Fig. 5). In the observations, nitrate (NO₃⁻) and phosphate (PO₄³⁻) have clear west-east tilting slopes associated with the thermocline during JJA (Fig. 5a, f, and k). According to Radenac et al. (2020), this nutrient supply to the euphotic zone is mainly driven by vertical advection associated with upwelling while vertical diffusion and meridional advection contribute to shape and spread the Atlantic summer bloom. As shown in Figs. 2b and 5b, the NorESM1-CTL fails to simulate the observed equatorial thermocline gradient. Corresponding to the flat thermocline, the upwelling of nitrate and phosphate is suppressed in the central to eastern



260 basin (Fig. 5g and l). In addition, the amount of nutrients is overestimated in the west (35°W-30°W) between 60 and 100 m depths. The westward-shifting and weaker summer bloom of production might be attributable to this nutrient supply bias in NorESM1-CTL. The alleviation of the thermocline bias by the climatological physical bias correction leads to a better representation of the pumping of subsurface nutrients from the central to eastern basin (Fig. 5h and m). Similar improvement can be detected in NorESM2 simulations (Fig. 5i, j, n and o) resulting in a better seasonal cycle of the primary production, especially, the Atlantic summer bloom (Fig. 3i and j). In the two NorESM1 versions, the ocean subsurface is cooler and more abundant in nutrients than in NorESM2s, which could be associated with the difference in the ecosystem parameters, in addition to the ocean circulation, i.e., stronger Atlantic overturning circulation (Tjiputra et al., 2020).



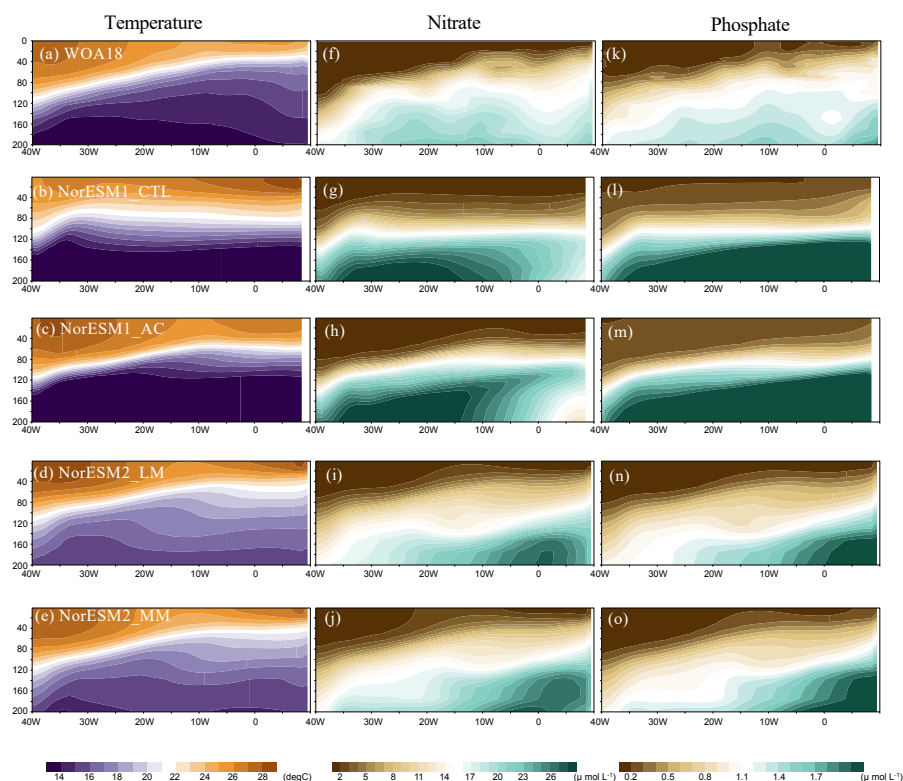
265

Figure 4: (a) Taylor diagram of the climatological seasonal cycle of SST (closed circle, primary production (closed square) and sea-air CO₂ flux (star) with respect to observation of OISST, MODIS, and MPI SOM-FFE, respectively. Each NorESM simulation is distinguished by different color (NorESM1-CTL: red, NorESM1-AC:blue, NorESM2-LM: green, NorESM2-MM: magenta). (b) Scatter plot between SST correlation coefficient and PP/CO₂ flux. The convention of color and marker is same as (a). Note that the standard deviation is normalized by that of observation and that the calculation of correlation and standard deviation do not include the data along the African coast.

270

275 Similar to the equatorial Atlantic, the climatologically-physical bias correction is beneficial for the coastal upwelling and nutrient supplies in the South Atlantic and western African coastal region where the marine biogeochemical cycle and ecosystem are very intense (Figs. S3 and S4, e.g., Cury and Shannon, 2004; Shannon et al., 2004). NorESM2-MM simulates better coastal upwelling and nutrients than NorESM2-LM indicating that the horizontal refinement of the atmospheric component is also beneficial for the coastal upwelling. While the improved nutrient supply can be effective for the primary production in the Benguela upwelling region (between 15°S and 35°S) in NorESM1-AC (Fig. S4), the primary

production in the Benguela upwelling region in the two NorESM2 simulations is greatly reduced compared to NorESM1-
280 CTL. This might be caused by the parameter tuning in biological dynamics processes that suppress the anomalously excess
primary production here and in other oceanic regions (Tjiputra et al., 2020). In contrast, NorESM2 has slightly more primary
production in the equatorial coastal region (between 5°S and 10°S) than NorESM1 (Fig. S4). This can be attributed to the
riverine-originated nutrient input from the Congo River implemented in NorESM2 (Gao et al., 2023; Tjiputra et al., 2020).



285

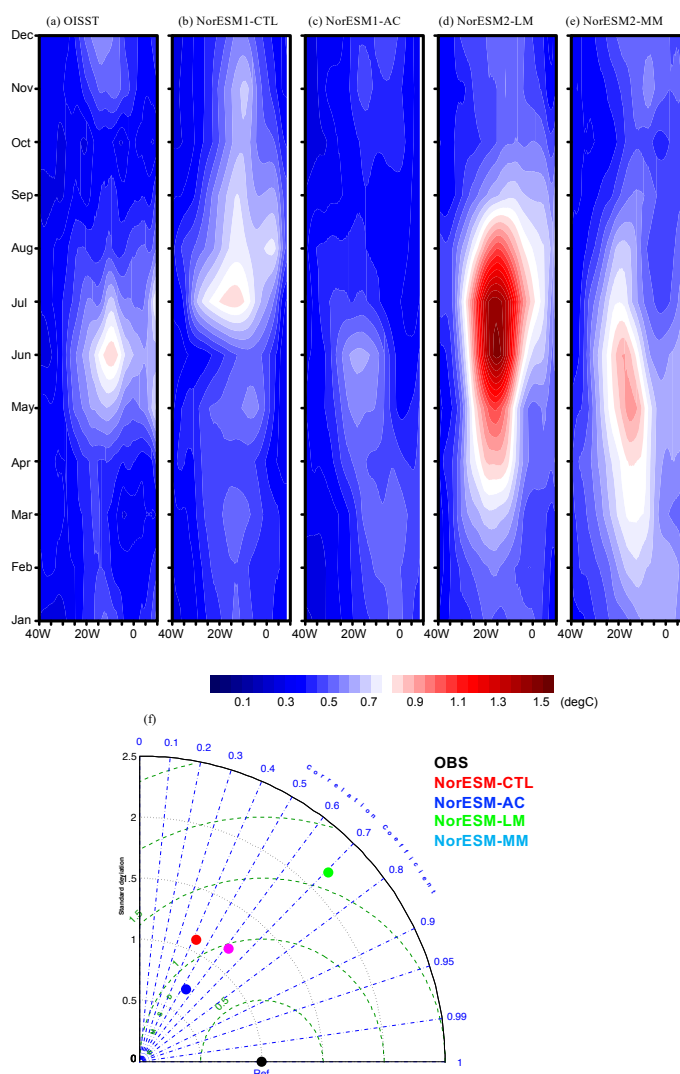
Figure 5: Depth-lonitudinal section of (left) temperature, (middle) nitrate, and (right) phosphate in JJA climatology for the observations and each NorESM simulation averaged over 3°S and 3°N.

3.3 Interannual variability

290 One of the most pronounced climate variability patterns in the tropical Atlantic is the Atlantic Zonal Mode (AZM; e.g., Keenlyside and Latif, 2007), referred as Atlantic Niño variability. As previous studies suggest (e.g., Counillon et al., 2021; Dippe et al., 2018), the climatological biases adversely affect the simulation of SST variability in the tropical Atlantic. In this section the Atlantic Niño variability and its impacts on the marine biogeochemical processes are assessed.

Figure 6a-e illustrates the seasonality of SST inter-annual variability along the equator. In the observations, the peak
295 of variability associated with the Atlantic Niño and Niña events is found from June to July at around 20°W (e.g., Dippe et al.,

2018; Nnamchi et al., 2015). Apart from the summer, there is a secondary peak during November to December (e.g., Okumura and Xie, 2006). NorESM1-CTL, to some extent, is able to reproduce the observed seasonality of SST variability, however its summer peak is delayed by one month and the winter peak appears one-month earlier in November (Fig. 6b). During the autumn, the variability is unrealistically strong compared to the observations. In contrast, NorESM1-AC is successful in simulating the summer and winter peaks with the right timing although the amplitude is weaker (Fig. 6c). Another study suggests that this improvement of variability is attributed to the improvement of the Bjerknes Feedback (e.g., Ding et al., 2015). While NorESM2-LM also reproduces the summer and winter peaks, this realization tends to overestimate



305 **Figure 6:** (a)-(e) same as in Fig. 3, but for SST standard deviation along the equator. (f) Same as in Fig. 4, but for the SST standard deviation.



the inter-annual variability, particularly, in summer (Fig. 6d). NorESM2-MM is also able to improve the SST variability
 310 having an overestimated summer peak amplitude (but more moderate than NorESM2-LM) (Fig. 6e). It is noteworthy that the
 strong summer variability can also be seen in the eastern coast of the equatorial Atlantic in NorESM2-MM, which is
 observed but not simulated in other NorESM runs (Fig. 6a-d). The performance in simulating the seasonal cycle of the
 variability is summarized in a Taylor diagram in Fig. 6f. The physical bias correction and updated version of NorESM
 improve the SST variability with respect to the reference NorESM1-CTL in terms of seasonality (better correlation). While
 315 NorESM2 is better than NorESM1-AC in terms of correlation, NorESM2-LM has a higher RMSE due to too-strong
 amplitude of the summer peak.

To investigate the marine biogeochemical response to the AZM, the Atlantic Niño and Niña events are estimated by
 detrending the Atlantic 3 index (det-ATL3) defined as June-July SST anomalies averaged in 20°W-0° and 3°S and 3°N.
 From the det-ATL3, the Atlantic Niño and Niña are defined as the det-ATL3 larger and smaller than \pm one standard
 320 deviation. Note that $0.75 \times$ standard deviation is used as the threshold for observation. Since the monthly primary production
 data is only available from 2000 to 2019 and the Atlantic Niño/Niña tends to be weaker during these decades (e.g., Prigent et
 al., 2020), the lower threshold yields more events of Atlantic Niño and Niña events. The events in NorESM simulations are
 defined by the individual ensemble member's climatology and standard deviation. To emphasize the anomalies due to the
 Atlantic Niño, the difference in composite between Atlantic Niño and Niña are shown and the values of composite anomalies
 325 are scaled by ATL3 index in the observation and simulations.

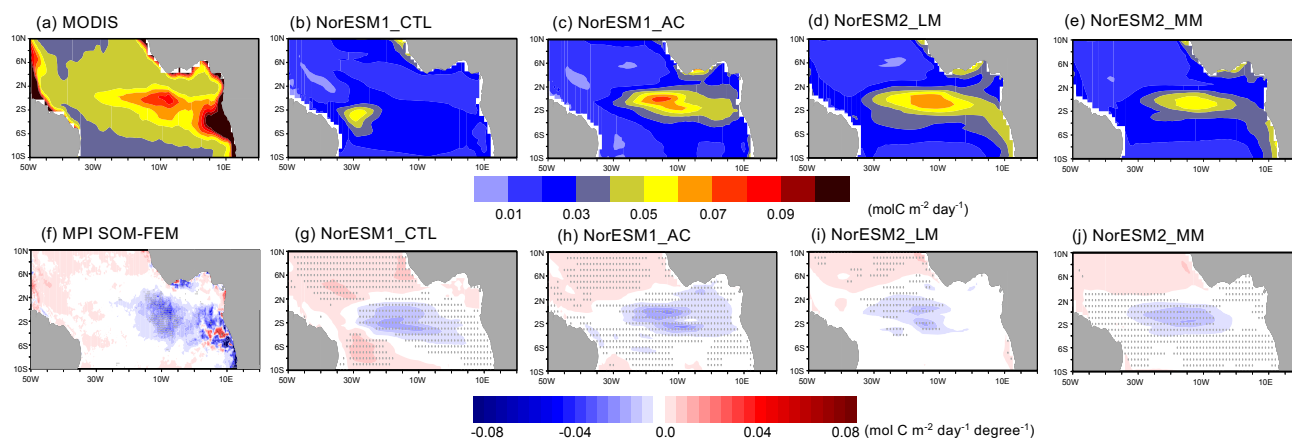


Figure 7: June-July-mean primary production for (top) climatology and (bottom) composite anomalies between Atlantic Niño and Niña
 for the observations and each NorESM simulation. The composite anomalies are scaled by ATL3-index anomalies between Atlantic Niño
 and Niña. Grey dots denote significance level of 90% estimated by Student's *t*-test.



In the observed climatology in June and July, the high productivity extends from the African coast to the equatorial Atlantic (Fig. 7a, see also Fig. 3f). The primary production is suppressed during the Atlantic Niño around 15°W to 10° W at the equator (Fig. 7f) (around the African coast, there are stronger but less significant anomalies). Chenillat et al. (2021) suggested that chlorophyll-*a* variability is driven mainly by the upwelling associated with Atlantic Niño and the corresponding nitrate supply from the ocean subsurface. NorESM1-CTL fails to reproduce the observed climatological Atlantic summer bloom and the maximum of primary production located closely to the northeastern Brazilian coast with a smaller magnitude (Fig. 7b). The strong suppression of the primary production during Atlantic Niño is located erroneously around 20°W, which is relatively westward from the observation (Figs. 7f and g). As shown in Fig. S5, the primary production anomaly during the Atlantic Niño is much worse than those during the Atlantic Niña. With the physical bias correction, the core of the Atlantic summer bloom is located in the central equatorial Atlantic (Fig. 7c) and the reduced primary production anomaly have a peak around 10°W, which is more realistic, in NorESM1-AC (Fig. 7h). Compared to NorESM1-CTL, the climatology and ATL3-scaled response of primary production is larger in NorESM1-AC, which is more in line with the observation (Fig. 7g and h). NorESM2 configurations also simulate the summer bloom at the more realistic location elongating from the eastern to central basin although the magnitude of the bloom is underestimated (Fig. 7d and e). In addition, there is some productivity (much smaller than the observation) along the western African coast (5°S to 10°S) that NorESM1s fail to reproduce. This could be associated with the riverine flux implemented in NorESM2s (Tjiputra et al., 2020). The suppression of primary production associated with the Atlantic Niño is well captured in the central basin (20°-10°W) at the equator, but its amplitude in NorESM2-LM is relatively smaller than NorESM1-AC (Fig. 7i). In NorESM2-MM, the climatological primary production is better reproduced with a larger amplitude than that of NorESM2-LM (Fig. 7d and e). The suppression of primary production is captured in the central basin at the equator during the Atlantic Niños (Fig. 7j).

As Chenillat et al. (2021) showed, the primary production during the summer fluctuates predominantly due to anomalous upwelling, modulating the nutrient supply from the subsurface, associated with the Atlantic Niño and Niña events. In NorESM1-CTL, the supply of nitrate is reduced during the Atlantic Niño consistent with the suppressed primary production and the anomaly minimum is centered around 100 m depth and 20°W (Fig. 8a). These upwelling-induced nitrate anomalies largely drive the simulated primary production anomalies. Compared to NorESM1-CTL, the nitrate anomalies shift shallower and eastward in NorESM1-AC (Fig. 8b). The negative anomalies crop up just below the ocean surface (~40 to 20m) in the central to eastern basin (20°W to 10°E), which is unclearly seen in NorESM1-CTL. This eastward shift and shoaling of nitrate anomalies appear to be important to produce more comparable primary production anomalies with the observations in NorESM1-AC than in NorESM1-CTL (Fig. 7g and h; e.g., the primary production in the model occurs in the euphotic zone fixed to the top 100m depth). Similarly, the shallower nitrate anomalies in NorESM2s are located in the central to eastern basin in Fig. 8c and d. Outcropping of the nitrate anomalies to the near-surface is also detected and



365 consequently, the primary production anomalies are comparable with the observations, especially in terms of location (Fig. 7i and j).

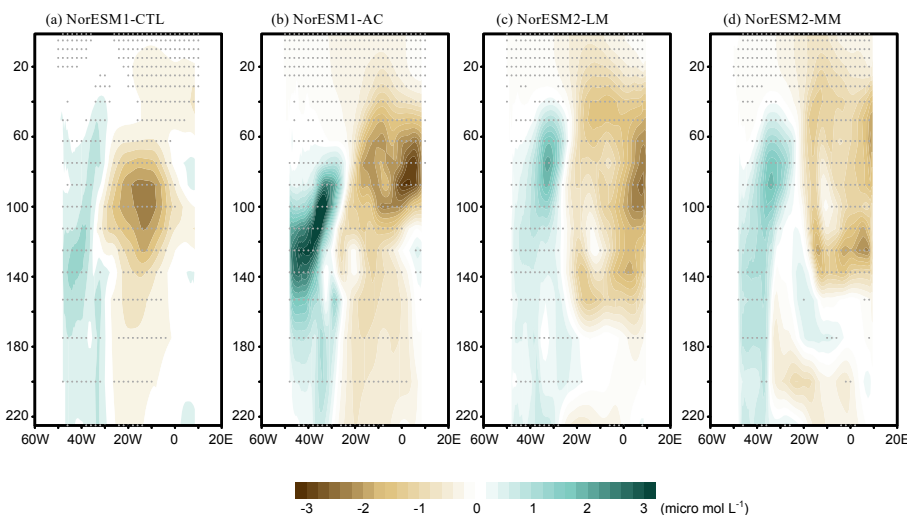


Figure 8: Depth-longitudinal sector (averaged between 3°S and 3°N) of June-July-mean composite anomalies of nitrate concentration between Atlantic Niño and Atlantic Niña in each NorESM simulation. Gray dots denote a significance level of 90% by Student's *t*-test.

370

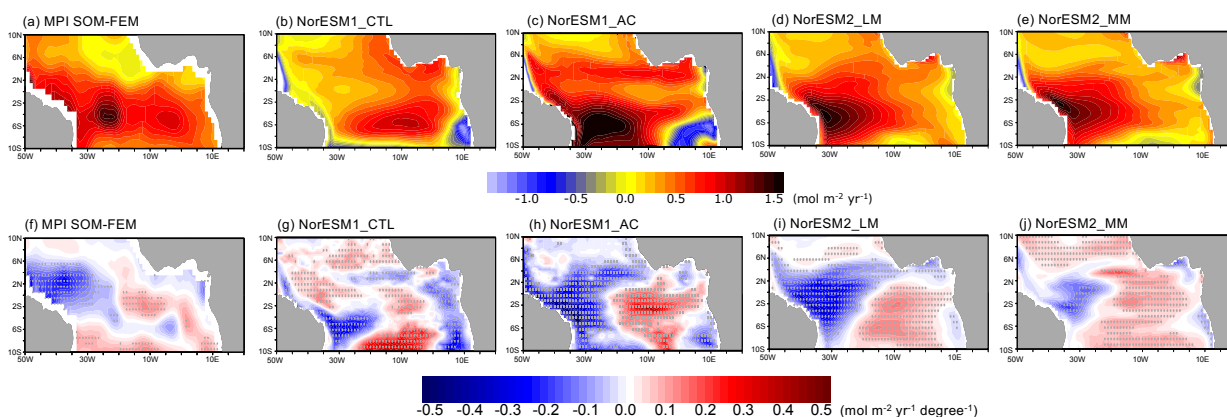
The observation shows that the climatological outgassing (ocean-to-atmosphere) CO_2 maximum is located in the western basin of the equatorial Atlantic and another moderate peak is detected in the central basin (Fig. 9a). As Koseki et al. (2023) showed, the CO_2 flux responds to the Atlantic Niños with a dipole structure in the equatorial Atlantic (Fig. 9f): The CO_2 outgassing is reduced during the Atlantic Niños around the northeastern Brazil coast (50°W-30°W), away from the core of SST anomalies (Fig. 6a and (Koseki, 2023)). Contrastingly, the CO_2 outgassing is enhanced in the central to eastern basin during the Atlantic Niños. According to Koseki et al. (2023), this dipole structure of anomalies is induced mainly by freshwater (western basin) and SST anomalies (central to eastern basin), which change the surface partial pressure of CO_2 . The spatial CO_2 flux pattern in NorESM1-CTL is largely biased, as shown in Fig. 9b. The climatological flux has its outgassing peak in the central basin more southward and there is a weak CO_2 uptake around the northeastern coast of Brazil (Fig. 9b). An ingassing bias is simulated along the African coast between 10°S and 6°S. NorESM1-CTL also fails to reproduce the spatial pattern of flux anomalies associated with the Atlantic Niños (Fig. 9g). The observed dipole structure of CO_2 flux anomalies during the Atlantic Niño is incorrectly simulated off the equator between 35°W and 0° at 6°S (Fig. 9f).

The climatological physical bias correction approach implemented in NorESM1-AC is somewhat successful in improving the climatological summer sea-air CO_2 flux in Fig. 9c. Although it is overestimated and the maximum of outgassing shifts southward compared to the observations, the strong upward CO_2 flux occurs more realistically in the western basin (Fig. 9c). The uptake bias remains along the west African coast indicating that the CO_2 flux variability here is not predominantly driven by SST, but rather by the bias in the biogeochemical properties or by the lack of riverine flux. The

385



Atlantic-Niño-induced CO₂ flux anomalies are generated more realistically along the equator having dipole structures and comparable amplitudes with the observations while their locations are still slightly southward (Fig. 9h). The two versions of
390 NorESM2 are also successful in simulating the climatological summer CO₂ flux in the tropical Atlantic (Fig. 9d and e): the maximum of outgassing CO₂ flux is located between 6°S and 0°, which is almost identical with the observations (Fig. 9a) and its amplitude is also more realistic (~1.5 mol C m⁻² yr⁻¹) than NorESM1-AC (Fig. 9c). Additionally, the NorESM2 configurations can alleviate ingassing bias along the African coast as well. The dipole pattern of CO₂ flux anomalies is also broadly represented along the equator in NorESM2s (Fig. 9i and j).



395

Figure 9: June-July-mean surface CO₂ flux for (top) climatology, and (bottom) composite anomalies between Atlantic Niño and Atlantic Niña for the observations and each NorESM simulation. Outgassing is shown by positive value. The composite anomalies are scaled by ATL3-index anomalies between Atlantic Niño and Niña. Grey dots denote a significance level of 90% estimated by Student's *t*-test.

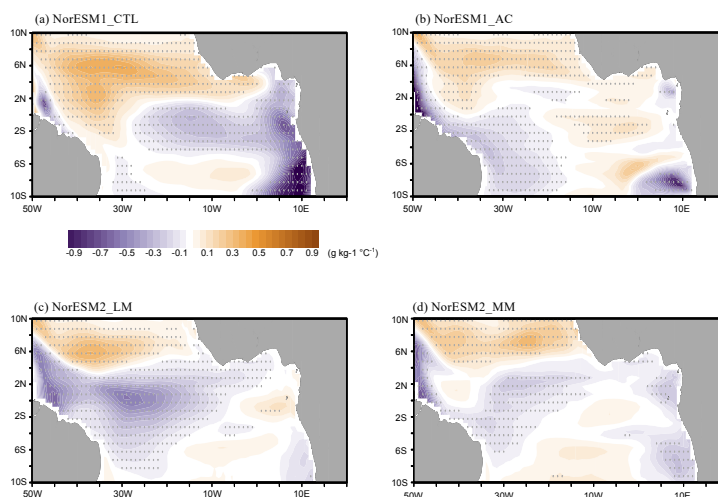
400

The surface ocean *p*CO₂ is one of the main driver of the sea-air CO₂ flux (e.g., Sarmiento, 2006). In NorESM1-CTL, the SSS negative anomaly is found in the central to eastern basin during Atlantic Niño covering the ACT whereas the positive anomaly occurs in the north tropical Atlantic (Fig. 10a). This SSS anomaly pattern reflects the displacement of the ITCZ associated with the warm event at the equator. The CO₂ flux anomaly pattern appears to be roughly consistent with these SSS anomalies: in the western basin, the less (more) CO₂ outgassing corresponds to the negative (positive) SSS at 8°S-
405 6°S (2°N-4°N). A part of the negative SSS anomalies covering the ACT co-locates with the less CO₂ outflux (Fig. 9g).

In NorESM1-AC, the negative SSS anomaly is found mainly in the western basin along the northeastern Brazilian coast and the positive SSS anomaly occurs northward of the negative SSS anomaly (Fig. 10b). As in NorESM1-CTL, this SSS anomaly pattern is associated with the ITCZ southward displacement, but the SSS anomalies are more dominant in the western basin in NorESM1-AC resulting in the less outgassing anomalies of CO₂ flux in the western basin, which is more
410 realistic (Figs. 9f and h). This difference in the ITCZ displacement and corresponding SST anomalies derive from the realistic development of the ACT during summer between NorESM1-CTL and NorESM1-AC (Fig. S2). In NorESM1-CTL, the ACT hardly develops and the climatological ITCZ is anchored more southward than the observation (e.g., Koseki et al.,



2018) and consequently, the ITCZ is perturbed by the Atlantic Niño around the equator. In the two NorESM2 versions, the SSS negative anomalies are also dominated in the western basin (Figs. 10c and d) and the CO₂ flux is correspondingly reduced in the western basin at the equator (Figs. 9i and j). Both NorESM2 simulations also reproduce the summer ACT development more realistically than NorESM1-CTL (Figs. S2c and d) and the freshwater anomalous inputs associated with the ITCZ displacement can be well captured resulting in the reduction of the CO₂ flux in the western basin.



420 **Figure 10:** June-July-mean composite anomalies of sea surface salinity for each NorESM simulation. The composite anomalies are scaled by ATL3-index anomalies between Atlantic Niño and Niña. Gray dots denote a significance level of 90% by Student's *t*-test.

4 Summary and Discussion

This study evaluated implications of physical bias on the simulated marine biogeochemical processes in the tropical Atlantic Ocean for 4 different realizations of the NorESM. A physical bias correction and better dynamical representations in new generation of NorESM improve the tropical Atlantic physical and biogeochemical biases during boreal summer, which are common in other ESMs (e.g., Voldoire et al., 2019). The seasonal development of the Atlantic Cold Tongue (ACT) is simulated more realistically during the boreal summer in NorESM1-AC and the NorESM2s than in the benchmark simulation of NorESM1-CTL. Associated with the better ACT development, the observed zonally-tilting thermocline is also well reproduced. NorESM2s can reproduce the shoaling in the eastern basin without any bias correction. This improvement of the thermocline gradient leads to a better representation of the observed nutrient supply from the subsurface in the eastern basin. Consequently, NorESM-AC and NorESM2s can simulate the observed timing (July to September) and location (centered at 10°W along the equator) of the Atlantic summer bloom of primary production. While NorESM2s include updates and tunings of physical and biogeochemical parameters relative to NorESM1s (e.g., Ilicak et al., 2008; Tjiputra et al., 2020; Toniazzo et al., 2020), NorESM1-AC only implements physical bias correction of surface wind and SST, which also resulted in remarkable improvements in its mean state and variability of biogeochemical processes. Our results



435 emphasize that atmospheric and ocean dynamics/physics are crucially important to simulate regional marine biogeochemical processes and their interaction in the tropical Atlantic (e.g., Berline et al., 2007; Fransner et al., 2020).

The benefit of physical bias correction can be especially seen along the Benguela upwelling region, where the highest biological production is observed in the tropical-subtropical Atlantic (e.g., (Shannon et al., 2004). With the physical bias correction, the high production area is confined along the Angola-Benguela coast, alleviating the initially
440 underestimated biological production (Fig. S4). This is attributed to the better upwelling and nutrients supply (Fig. S3) associated with the corrected coastal low-level jet and wind stress curl that are essential drivers of coastal upwelling (e.g., Koseki et al., 2018; Lima et al., 2019). Contrastingly, NorESM2s tend to degrade the coastal production in the southeast Atlantic. This might be due to the tunings of biological parameters to reduce the largely-overestimated production in other ocean areas (Tjiputra et al., 2020). However, due to the newly-implemented riverine flux (Gao et al., 2023), the primary
445 production is to some extent enhanced around the Congo river mouth (around 5°S) as compared to the NorESM1 (Fig. S4), which does not include riverine flux. Between NorESM2-LM and NorESM2-MM, the SST bias and nutrients upwelling biases are alleviated in NorESM2-MM where the atmospheric component resolution is finer than that in NorESM2-LM. The atmospheric refinement is beneficial to improve the model performance in reproducing the tropical Atlantic climate (Harlass et al., 2018).

450 With better representation of the physical processes, the interannual variability of biogeochemical processes is also improved. As Chenillat et al. (2021) showed, the Atlantic Niño is one of the essential drivers for variability in the primary production in the equatorial Atlantic. NorESM-AC and NorESM2s can reproduce the reduction of the summer bloom in the central basin while NorESM-CTL simulates the summer bloom anomaly in the wrong location. Because the primary production anomaly is mainly induced by the upwelling modulation associated with the Atlantic Niño (e.g., Chenillat et al.,
455 2021), a more realistic thermocline structure in NorESM-AC and NorESM2s is able to capture the observed summer bloom variations. The sea-air CO₂ flux anomalies associated with the Atlantic Niño are also more realistically reproduced in NorESM2-AC and NorESM2s than NorESM1-CTL. The CO₂ flux anomalies in the western basin is mainly driven by the SSS anomalies associated with the ITCZ displacement (Koseki et al., 2023) and this study suggests that the realistic representation of the ACT and ITCZ are responsible for simulating the observed CO₂ flux anomalies due to the Atlantic
460 Niño. We also note that in addition to proper physical representation, accurate representation of subsurface biogeochemical state is also crucial in reproducing the observed variability in an upwelling system such as the tropical Atlantic (e.g., Ayar et al., 2022; Koseki et al., 2023).

The physical bias is one of the main reasons why the climate prediction and projection are uncertain (e.g., Bethke et al., 2021; Counillon et al., 2021; Crespo et al., 2022). As we showed in this study, the physical bias reduction allows us to
465 reproduce more realistic marine biogeochemical processes by improving interaction between physics and biogeochemistry. Therefore, future improvements in biogeochemical processes and parameterization (Singh et al., 2022; Tjiputra et al., 2007) should also take into consideration biases in physical processes to avoid overfitting or correctly simulating biogeochemical processes but for wrong reason. Our study also highlights the importance of evaluating the Earth system models'



performance at regional scale and at timescale where natural climatic variability dominates over external forcing.
470 Improvements at these spatial and temporal scales are particularly valuable due to the more direct and significant impacts on
the society. Future model evaluation should go beyond capturing the large scale, mean state features and focus more on
regional dynamics across seasonal-to-decadal time scales.

Acknowledgement

This study is supported by the H2020 TRIATLAS project (grant# 817578). The observational data of SST and CO₂ flux are
475 available to download at <https://www.ncei.noaa.gov/products/optimum-interpolation-sst> and
https://www.ncei.noaa.gov/access/ocean-carbon-data-system/oceans/MPI-ULB-SOM_FFN_clim.html, respectively. The
computational resources of NorESM simulation and data archive are supported by UNINETT Sigma2 AS (NN9039K and
NS9560K).

Authors Contribution

480 SK and LRC have conducted NorESM1 simulations and conducted the analysis of the experiments. All the authors have
discussions on results and their interpretations. All the authors have contributed to build a manuscript and improve it to the
final form of the manuscript.

Data Availability

485 All data is available on request.

Code Availability

All codes are available on request.

References

490 Araujo, M., Noriega, C., and Lefevre, N.: Nutrients and carbon fluxes in the estuaries of major rivers flowing into the
tropical Atlantic. *Frontiers in Marine Science*, 1. <https://doi.org/ARTN> 10, 10.3389/fmars.2014.00010, 2014.
Ayar, P. V., Bopp, L., Christian, J. R., Ilyina, T., Krasting, J. P., Seferian, R., Tsujino, H., Watanabe, M., Yool, A., and
Tjiputra, J.: Contrasting projections of the ENSO-driven CO₂ flux variability in the equatorial Pacific under high-
warming scenario. *Earth System Dynamics*, 13(3), 1097-1118. <https://doi.org/10.5194/esd-13-1097-2022>, 2022



- 495 Bentsen, M., Bethke, I., Debernard, J. B., Iversen, T., Kirkevag, A., Seland, O., Drange, H., Roelandt, C., Seierstad, I. A.,
Hoose, C., and Kristjansson, J. E.: The Norwegian Earth System Model, NorESM1-M - Part 1: Description and
basic evaluation of the physical climate. *Geoscientific Model Development*, 6(3), 687-720.
<https://doi.org/10.5194/gmd-6-687-2013>, 2013.
- 500 Berline, L., Brankart, J. M., Brasseur, P., Ourmieres, Y., and Verron, J.: Improving the physics of a coupled physical-
biogeochemical model of the North Atlantic through data assimilation: Impact on the ecosystem. *Journal of Marine
Systems*, 64(1-4), 153-172. <https://doi.org/10.1016/j.jmarsys.2006.03.007>, 2007.
- Bertini, L., and Tjiputra, J.: Biogeochemical Timescales of Climate Change Onset and Recovery in the North Atlantic
Interior Under Rapid Atmospheric CO₂ Forcing. *Journal of Geophysical Research-Oceans*, 127(4).
<https://doi.org/ARTN> e2021JC017929, 10.1029/2021JC017929, 2022.
- 505 Bethke, I., Wang, Y. G., Counillon, F., Keenlyside, N., Kimmritz, M., Fransner, F., Samuelsen, A., Langehaug, H.,
Svendsen, L., Chiu, P. G., Passos, L., Bentsen, M., Guo, C. C., Gupta, A., Tjiputra, J., Kirkevag, A., Olivie, D.,
Seland, O., Vagane, J. S., . . . Eldevik, T.: NorCPM1 and its contribution to CMIP6 DCP. *Geoscientific Model
Development*, 14(11), 7073-7116. <https://doi.org/10.5194/gmd-14-7073-2021>, 2021.
- Bjerknes, J.: Atmospheric Teleconnections from Equatorial Pacific. *Monthly Weather Review*, 97(3), 163-and.
<https://doi.org/Doi> 10.1175/1520-0493(1969)097<0163:Atftep>2.3.Co;2, 1969.
- 510 Bleck, R., Rooth, C., Hu, D. M., and Smith, L. T.: Salinity-Driven Thermocline Transients in a Wind-Forced and
Thermohaline-Forced Isopycnic Coordinate Model of the North-Atlantic. *Journal of Physical Oceanography*,
22(12), 1486-1505. <https://doi.org/Doi> 10.1175/1520-0485(1992)022<1486:Sdtia>2.0.Co;2, 1992.
- Bouillon, S., Yambele, A., Spencer, R. G. M., Gillikin, D. P., Hernes, P. J., Six, J., Merckx, R., and Borges, A. V.: Organic
matter sources, fluxes and greenhouse gas exchange in the Oubangui River (Congo River basin). *Biogeosciences*,
515 9(6), 2045-2062. <https://doi.org/10.5194/bg-9-2045-2012>, 2012.
- Bourgeois, T., Goris, N., Schwinger, J., and Tjiputra, J. F.: Stratification constrains future heat and carbon uptake in the
Southern Ocean between 30 degrees S and 55 degrees S. *Nature Communications*, 13(1). <https://doi.org/ARTN> 340,
10.1038/s41467-022-27979-5, 2022.
- 520 Cabos, W., Sein, D. V., Pinto, J. G., Fink, A. H., Koldunov, N. V., Alvarez, F., Izquierdo, A., Keenlyside, N., and Jacob, D.:
The South Atlantic Anticyclone as a key player for the representation of the tropical Atlantic climate in coupled
climate models. *Climate Dynamics*, 48(11), 4051-4069. <https://doi.org/10.1007/s00382-016-3319-9>, 2017.
- Chenillat, F., Illig, S., Jouanno, J., Awo, F. M., Alory, G., and Brehmer, P.: How do Climate Modes Shape the Chlorophyll-a
Interannual Variability in the Tropical Atlantic? *Geophysical Research Letters*, 48(14). <https://doi.org/ARTN>
e2021GL093769, 10.1029/2021GL093769, 2021.
- 525 Counillon, F., Keenlyside, N., Toniazzo, T., Koseki, S., Demissie, T., Bethke, I., and Wang, Y. G.: Relating model bias and
prediction skill in the equatorial Atlantic. *Climate Dynamics*, 56(7-8), 2617-2630. <https://doi.org/10.1007/s00382-020-05605-8>, 2021.
- Crespo, L. R., Keenlyside, N., and Koseki, S.: The role of sea surface temperature in the atmospheric seasonal cycle of the
equatorial Atlantic. *Climate Dynamics*, 52(9-10), 5927-5946. <https://doi.org/10.1007/s00382-018-4489-4>, 2019.
- 530 Crespo, L. R., Prigent, A., Keenlyside, N., Koseki, S., Svendsen, L., Richter, I., and Sánchez-Gómez, E.: Weakening of the
Atlantic Niño variability under global warming. *Nature Climate Change*, 12, 822-827,
<https://doi.org/10.1038/s41558-022-01453-y>, 2022
- Cury, P., and Shannon, L.: Regime shifts in upwelling ecosystems: observed changes and possible mechanisms in the
northern and southern Benguela. *Progress in Oceanography*, 60(2-4), 223-243.
535 <https://doi.org/10.1016/j.pocean.2004.02.007>, 2004.
- de la Vara, A., Cabos, W., Sein, D. V., Sidorenko, D., Koldunov, N. I. V., Koseki, S., Soares, P. M. M., and Danilov, S.: On
the impact of atmospheric vs oceanic resolutions on the representation of the sea surface temperature in the South
Eastern Tropical Atlantic. *Climate Dynamics*, 54(11-12), 4733-4757. <https://doi.org/10.1007/s00382-020-05256-9>,
2020.
- 540 Dee, D. P., Uppala, S. M., Simmons, A. J., Berrisford, P., Poli, P., Kobayashi, S., Andrae, U., Balmaseda, M. A., Balsamo,
G., Bauer, P., Bechtold, P., Beljaars, A. C. M., van de Berg, L., Bidlot, J., Bormann, N., Delsol, C., Dragani, R.,
Fuentes, M., Geer, A. J., . . . Vitart, F.: The ERA-Interim reanalysis: configuration and performance of the data



- assimilation system. *Quarterly Journal of the Royal Meteorological Society*, 137(656), 553-597. <https://doi.org/10.1002/qj.828>, 2011.
- 545 Demaster, D. J., and Pope, R. H.: Nutrient dynamics in Amazon shelf waters: Results from AMASSEDs. *Continental Shelf Research*, 16(3), 263-289. [https://doi.org/10.1016/0278-4343\(95\)00008-O](https://doi.org/10.1016/0278-4343(95)00008-O), 1996.
- Deppenmeier, A. L., Haarsma, R. J., LeSager, P., and Hazeleger, W.: The effect of vertical ocean mixing on the tropical Atlantic in a coupled global climate model. *Climate Dynamics*, 54(11-12), 5089-5109. <https://doi.org/10.1007/s00382-020-05270-x>, 2020.
- 550 Ding, H., Keenlyside, N., Latif, M., Park, W., and Wahl, S.: The impact of mean state errors on equatorial Atlantic interannual variability in a climate model. *Journal of Geophysical Research-Oceans*, 120(2), 1133-1151. <https://doi.org/10.1002/2014jc010384>, 2015.
- Ding, H., Keenlyside, N. S., and Latif, M.: Seasonal cycle in the upper equatorial Atlantic Ocean. *Journal of Geophysical Research-Oceans*, 114. <https://doi.org/10.1029/2009jc005418>, 2009.
- 555 Dippe, T., Greatbatch, R. J., and Ding, H.: On the relationship between Atlantic Nio variability and ocean dynamics. *Climate Dynamics*, 51(1-2), 597-612. <https://doi.org/10.1007/s00382-017-3943-z>, 2018.
- Doney, S. C.: Major challenges confronting marine biogeochemical modeling. *Global Biogeochemical Cycles*, 13(3), 705-714. <https://doi.org/10.1029/1999gb900039>, 1999.
- 560 Eyring, V., Bony, S., Meehl, G. A., Senior, C. A., Stevens, B., Stouffer, R. J., and Taylor, K. E.: Overview of the Coupled Model Intercomparison Project Phase 6 (CMIP6) experimental design and organization. *Geoscientific Model Development*, 9(5), 1937-1958. <https://doi.org/10.5194/gmd-9-1937-2016>, 2016.
- Fransner, F., Counillon, F., Bethke, I., Tjiputra, J., Samuelsen, A., Nummelin, A., and Olsen, A.: Ocean Biogeochemical Predictions-Initialization and Limits of Predictability. *Frontiers in Marine Science*, 7. <https://doi.org/10.3389/fmars.2020.00386>, 2020.
- 565 Gao, S., Schwinger, J., Tjiputra, J., Bethke, I., Hartmann, J., Mayorga, E., and Heinze, C.: Riverine impact on future projections of marine primary production and carbon uptake. *Biogeosciences*, 20(1), 93-119. <https://doi.org/10.5194/bg-20-93-2023>, 2023.
- Goris, N., Johannsen, K., and Tjiputra, J.: The emergence of the Gulf Stream and interior western boundary as key regions to constrain the future North Atlantic carbon uptake. *Geoscientific Model Development*, 16(8), 2095-2117. <https://doi.org/10.5194/gmd-16-2095-2023>, 2023.
- 570 Goris, N., Tjiputra, J. F., Olsen, A., Schwinger, J., Lauvset, S. K., and Jeansson, E.: Constraining Projection-Based Estimates of the Future North Atlantic Carbon Uptake. *Journal of Climate*, 31(10), 3959-3978. <https://doi.org/10.1175/JCLI-D-17-0564.1>, 2018.
- 575 Gregg, W. W., Conkright, M. E., Ginoux, P., O'Reilly, J. E., and Casey, N. W.: Ocean primary production and climate: Global decadal changes. *Geophysical Research Letters*, 30(15). <https://doi.org/10.1029/2003gl016889>, 2003.
- Harlass, J., Latif, M., and Park, W.: Alleviating tropical Atlantic sector biases in the Kiel climate model by enhancing horizontal and vertical atmosphere model resolution: climatology and interannual variability. *Climate Dynamics*, 50(7-8), 2605-2635. <https://doi.org/10.1007/s00382-017-3760-4>, 2018.
- 580 Hummels, R., Dengler, M., and Bourles, B.: Seasonal and regional variability of upper ocean diapycnal heat flux in the Atlantic cold tongue. *Progress in Oceanography*, 111, 52-74. <https://doi.org/10.1016/j.pocean.2012.11.001>, 2013.
- Hutchings, L., van der Linden, C. D., Shannon, L. J., Crawford, R. J. M., Verheye, H. M. S., Bartholomae, C. H., van der Plas, A. K., Louw, D., Kreiner, A., Ostrowski, M., Fidel, Q., Barlow, R. G., Lamont, T., Coetzee, J., Shillington, F., Veitch, J., Currie, J. C., and Monteiro, P. M. S.: The Benguela Current: An ecosystem of four components. *Progress in Oceanography*, 83(1-4), 15-32. <https://doi.org/10.1016/j.pocean.2009.07.046>, 2009.
- 585 Ilicak, M., Ozgokmen, T. M., Peters, H., Baumert, H. Z., and Iskandarani, M.: Performance of two-equation turbulence closures in three-dimensional simulations of the Red Sea overflow. *Ocean Modelling*, 24(3-4), 122-139. <https://doi.org/10.1016/j.ocemod.2008.06.001>, 2008.
- 590 Ilyina, T., Six, K. D., Segschneider, J., Maier-Reimer, E., Li, H. M., and Nunez-Riboni, I.: Global ocean biogeochemistry model HAMOCC: Model architecture and performance as component of the MPI-Earth system model in different



- CMIP5 experimental realizations. *Journal of Advances in Modeling Earth Systems*, 5(2), 287-315. <https://doi.org/10.1029/2012ms000178>, 2013.
- 595 Kawase, M., and Sarmiento, J. L.: Nutrients in the Atlantic Thermocline. *Journal of Geophysical Research-Oceans*, 90(Nc5), 8961-8979. [https://doi.org/DOI 10.1029/JC090iC05p08961](https://doi.org/DOI%2010.1029/JC090iC05p08961), 1985.
- Keenlyside, N. S., and Latif, M.: Understanding equatorial Atlantic interannual variability. *Journal of Climate*, 20(1), 131-142. <https://doi.org/10.1175/Jcli3992.1>, 2007.
- Koseki, S., Giordani, H., and Goubanova, K.: Frontogenesis of the Angola-Benguela Frontal Zone. *Ocean Science*, 15(1), 83-96. <https://doi.org/10.5194/os-15-83-2019>, 2019.
- 600 Koseki, S., Keenlyside, N., Demissie, T., Toniazzo, T., Counillon, F., Bethke, I., Ilıcak, M., and Shen, M. L.: Causes of the large warm bias in the Angola-Benguela Frontal Zone in the Norwegian Earth System Model. *Climate Dynamics*, 50(11-12), 4651-4670. <https://doi.org/10.1007/s00382-017-3896-2>, 2018.
- Koseki, S., Tjiputra, J., Fransner, F., Crespo, L.R., Keenlyside, N. S.: Disentangling the impact of Atlantic Niño on sea-air CO₂ flux. *Nature Communications*, 14, 3649, <https://doi.org/19.1038/s41467-023-38718-9>, 2023.
- 605 Kriest, I., and Oschlies, A.: MOPS-1.0: towards a model for the regulation of the global oceanic nitrogen budget by marine biogeochemical processes. *Geoscientific Model Development*, 8(9), 2929-2957. <https://doi.org/10.5194/gmd-8-2929-2015>, 2015.
- Landschutzer, P., Gruber, N., and Bakker, D. C. E.: Decadal variations and trends of the global ocean carbon sink. *Global Biogeochemical Cycles*, 30(10), 1396-1417. <https://doi.org/10.1002/2015gb005359>, 2016.
- 610 Landschutzer, P., Laruelle, G. G., Roobaert, A., and Regnier, P.: A uniform pCO₂ climatology combining open and coastal oceans. *Earth System Science Data*, 12(4), 2537-2553. <https://doi.org/10.5194/essd-12-2537-2020>, 2020.
- Lefevre, N., Caniaux, G., Janicot, S., and Gueye, A. K.: Increased CO₂ outgassing in February-May 2010 in the tropical Atlantic following the 2009 Pacific El Niño. *Journal of Geophysical Research-Oceans*, 118(4), 1645-1657. <https://doi.org/10.1002/jgrc.20107>, 2013.
- 615 Lima, D. C. A., Soares, P. M. M., Semedo, A., Cardoso, R. M., Cabos, W., and Sein, D. V.: A Climatological Analysis of the Benguela Coastal Low-Level Jet. *Journal of Geophysical Research-Atmospheres*, 124(7), 3960-3978. <https://doi.org/10.1029/2018jd028944>, 2019.
- Menard, F., Fonteneau, A., Gaertner, D., Nordstrom, V., Stequert, B., and Marchal, E.: Exploitation of small tunas by a purse-seine fishery with fish aggregating devices and their feeding ecology in an eastern tropical Atlantic ecosystem. *ICES Journal of Marine Science*, 57(3), 525-530. [https://doi.org/DOI 10.1006/jmsc.2000.0717](https://doi.org/DOI%2010.1006/jmsc.2000.0717), 2000.
- 620 Mohino, E., Rodriguez-fonseca, B., Mechoso, C. R., Losada, T., and Polo, I.: Relationships among Intermodel Spread and Biases in Tropical Atlantic Sea Surface Temperatures. *Journal of Climate*, 32(12), 3615-3635. <https://doi.org/10.1175/Jcli-D-18-0846.1>, 2019.
- Moreira-Turcq, P., Seyler, P., Guyot, J. L., and Etcheber, H.: Exportation of organic carbon from the Amazon River and its main tributaries. *Hydrological Processes*, 17(7), 1329-1344. <https://doi.org/10.1002/hyp.1287>, 2003.
- 625 Neale, R. B., Richter, J. H., Conley, A. J., Park, S., Lauritzen, P. H., Gettleman, A., Williamson, D. L., Rasch, P. J., Vavrus, S. J., Taylor, M. A., Collins, W. D., Zhang, M., and Lin, S.-J.: Description of the NCAR Community Atmosphere Model (CAM 4.09); . *Tech. Rep., NCAR/TN-485+STR*, 2010.
- Nnamchi, H. C., Latif, M., Keenlyside, N. S., Kjellsson, J., and Richter, I.: Diabatic heating governs the seasonality of the Atlantic Niño. *Nature Communications*, 12(1). [https://doi.org/ARTN 376](https://doi.org/ARTN%20376), 10.1038/s41467-020-20452-1, 2021.
- 630 Nnamchi, H. C., Li, J. P., Kucharski, F., Kang, I. S., Keenlyside, N. S., Chang, P., and Farneti, R.: Thermodynamic controls of the Atlantic Niño. *Nature Communications*, 6. [https://doi.org/ARTN 8895](https://doi.org/ARTN%208895), 10.1038/ncomms9895, 2015.
- Okumura, Y., and Xie, S. P.: Some overlooked features of tropical Atlantic climate leading to a new Niño-like phenomenon. *Journal of Climate*, 19(22), 5859-5874. [https://doi.org/Doi 10.1175/Jcli3928.1](https://doi.org/Doi%2010.1175/Jcli3928.1), 2006.
- 635 Perez, V., Fernandez, E., Maranon, E., Serret, P., and Garcia-Soto, C.: Seasonal and interannual variability of chlorophyll a and primary production in the Equatorial Atlantic: in situ and remote sensing observations. *Journal of Plankton Research*, 27(2), 189-197. <https://doi.org/10.1093/plankt/fbh159>, 2005.
- Prigent, A., Lubbecke, J. F., Bayr, T., Latif, M., and Wengel, C.: Weakened SST variability in the tropical Atlantic Ocean since 2000. *Climate Dynamics*, 54(5-6), 2731-2744. <https://doi.org/10.1007/s00382-020-05138-0>, 2020.



- 640 Prodhomme, C., Voldoire, A., Exarchou, E., Deppenmeier, A. L., Garcia-Serrano, J., and Guemas, V.: How Does the Seasonal Cycle Control Equatorial Atlantic Interannual Variability? *Geophysical Research Letters*, 46(2), 916-922. <https://doi.org/10.1029/2018gl080837> , 2019.
- Radenac, M. H., Jouanno, J., Tchamabi, C. C., Awo, M., Bourles, B., Arnault, S., and Aumont, O.: Physical drivers of the nitrate seasonal variability in the Atlantic cold tongue. *Biogeosciences*, 17(2), 529-545. <https://doi.org/10.5194/bg-17-529-2020> , 2020.
- 645 Ramirez-Romero, E., Jorda, G., Amores, A., Kay, S., Segura-Noguera, M., Macias, D. M., Maynou, F., Sabates, A., and Catalan, I. A.: Assessment of the Skill of Coupled Physical-Biogeochemical Models in the NW Mediterranean. *Frontiers in Marine Science*, 7. <https://doi.org/ARTN> 497, 10.3389/fmars.2020.00497 , 2020.
- Reynolds, R. W., Smith, T. M., Liu, C., Chelton, D. B., Casey, K. S., and Schlax, M. G.: Daily high-resolution-blended analyses for sea surface temperature. *Journal of Climate*, 20(22), 5473-5496. <https://doi.org/10.1175/2007jcli1824.1> , 2007.
- Richter, I.: Climate model biases in the eastern tropical oceans: causes, impacts and ways forward. *Wiley Interdisciplinary Reviews-Climate Change*, 6(3), 345-358. <https://doi.org/10.1002/wcc.338> , 2015.
- Richter, I., Behera, S. K., Masumoto, Y., Taguchi, B., Sasaki, H., and Yamagata, T.: Multiple causes of interannual sea surface temperature variability in the equatorial Atlantic Ocean. *Nature Geoscience*, 6(1), 43-47. <https://doi.org/10.1038/Ngeo1660> , 2013.
- 655 Santos, A. M. P., Chicharo, A., Dos Santos, A., Moita, T., Oliveira, P. B., Peliz, A., and Re, P.: Physical-biological interactions in the life history of small pelagic fish in the Western Iberia Upwelling Ecosystem. *Progress in Oceanography*, 74(2-3), 192-209. <https://doi.org/10.1016/j.pocean.2007.04.008> , 2007.
- 660 Sarmiento, J. L., Gruber, N.: *Ocean Biogeochemical Dynamics*. Princeton University Press. , 2006.
- Seferian, R., Berthet, S., and Chevallier, M.: Assessing the Decadal Predictability of Land and Ocean Carbon Uptake. *Geophysical Research Letters*, 45(5), 2455-2466. <https://doi.org/10.1002/2017gl076092> , 2018.
- Seferian, R., Berthet, S., Yool, A., Palmieri, J., Bopp, L., Tagliabue, A., Kwiatkowski, L., Aumont, O., Christian, J., Dunne, J., Gehlen, M., Ilyina, T., John, J. G., Li, H. M., Long, M. C., Luo, J. Y., Nakano, H., Romanou, A., Schwinger, J., . . . Yamamoto, A.: Tracking Improvement in Simulated Marine Biogeochemistry Between CMIP5 and CMIP6. *Current Climate Change Reports*, 6(3), 95-119. <https://doi.org/10.1007/s40641-020-00160-0> , 2020.
- 665 Seferian, R., Nabat, P., Michou, M., Saint-Martin, D., Voldoire, A., Colin, J., Decharme, B., Delire, C., Berthet, S., Chevallier, M., Senesi, S., Franchisteguy, L., Vial, J., Mallet, M., Joetzjer, E., Geoffroy, O., Gueremy, J. F., Moine, M. P., Msadek, R., . . . Madec, G.: Evaluation of CNRM Earth System Model, CNRM-ESM2-1: Role of Earth System Processes in Present-Day and Future Climate. *Journal of Advances in Modeling Earth Systems*, 11(12), 4182-4227. <https://doi.org/10.1029/2019ms001791> , 2019.
- 670 Sein, D. V., Mikolajewicz, U., Groger, M., Fast, I., Cabos, W., Pinto, J. G., Hagemann, S., Semmler, T., Izquierdo, A., and Jacob, D.: Regionally coupled atmosphere-ocean-sea ice-marine biogeochemistry model ROM: 1. Description and validation. *Journal of Advances in Modeling Earth Systems*, 7(1), 268-304. <https://doi.org/10.1002/2014ms000357> , 2015.
- 675 Seland, O., Bentsen, M., Olivie, D., Toniazzo, T., Gjermundsen, A., Graff, L. S., Debernard, J. B., Gupta, A. K., He, Y. C., Kirkevag, A., Schwinger, J., Tjiputra, J., Aas, K. S., Bethke, I., Fan, Y. C., Griesfeller, J., Grini, A., Guo, C. C., Ilicak, M., . . . Schulz, M.: Overview of the Norwegian Earth System Model (NorESM2) and key climate response of CMIP6 DECK, historical, and scenario simulations. *Geoscientific Model Development*, 13(12), 6165-6200. <https://doi.org/10.5194/gmd-13-6165-2020> , 2020.
- 680 Shannon, L. J., Christensen, V., and Walters, C. J.: Modelling stock dynamics in the southern Benguela ecosystem for the period 1978-2002. *African Journal of Marine Science*, 26, 179-196. <https://doi.org/10.2989/18142320409504056> , 2004.
- Singh, T., Counillon, F., Tjiputra, J., Wang, Y. G., and Gharamti, M. E.: Estimation of Ocean Biogeochemical Parameters in an Earth System Model Using the Dual One Step Ahead Smoother: A Twin Experiment. *Frontiers in Marine Science*, 9. <https://doi.org/ARTN> 775394, 10.3389/fmars.2022.775394 , 2022.
- 685 Takahashi, T., Sutherland, S. C., Sweeney, C., Poisson, A., Metz, N., Tilbrook, B., Bates, N., Wanninkhof, R., Feely, R. A., Sabine, C., Olafsson, J., and Nojiri, Y.: Global sea-air CO₂ flux based on climatological surface ocean pCO₂(2), and



- 690 seasonal biological and temperature effects. *Deep-Sea Research Part Ii-Topical Studies in Oceanography*, 49(9-10),
1601-1622. [https://doi.org/Pii/S0967-0645\(02\)00003-6](https://doi.org/Pii/S0967-0645(02)00003-6), doi 10.1016/S0967-0645(02)00003-6 , 2002.
- Taylor, K. E., Stouffer, R. J., and Meehl, G. A.: An Overview of Cmp5 and the Experiment Design. *Bulletin of the
American Meteorological Society*, 93(4), 485-498. <https://doi.org/10.1175/Bams-D-11-00094.1> , 2012.
- Tjiputra, J., Negrel, J., Olsen, A.: Early detection of anthropogenic climate change signals in the ocean interior. *Scientific
Reports*, 13. <https://doi.org/https://doi.org/10.1038/s41598-023-30159-0> , 2023.
- 695 Tjiputra, J. F., Assmann, K., Bentsen, M., Bethke, I., Ottera, O. H., Sturm, C., and Heinze, C.: Bergen Earth system model
(BCM-C): model description and regional climate-carbon cycle feedbacks assessment. *Geoscientific Model
Development*, 3(1), 123-141. <https://doi.org/DOI/10.5194/gmd-3-123-2010> , 2010.
- Tjiputra, J. F., Polzin, D., and Winguth, A. M. E.: Assimilation of seasonal chlorophyll and nutrient data into an adjoint
three-dimensional ocean carbon cycle model: Sensitivity analysis and ecosystem parameter optimization. *Global
700 Biogeochemical Cycles*, 21(1). <https://doi.org/Artn/Gb1001>, 10.1029/2006gb002745 , 2007.
- Tjiputra, J. F., Roelandt, C., Bentsen, M., Lawrence, D. M., Lorentzen, T., Schwinger, J., Seland, O., and Heinze, C.:
Evaluation of the carbon cycle components in the Norwegian Earth System Model (NorESM). *Geoscientific Model
Development*, 6(2), 301-325. <https://doi.org/10.5194/gmd-6-301-2013> , 2013.
- Tjiputra, J. F., Schwinger, J., Bentsen, M., Moree, A. L., Gao, S., Bethke, I., Heinze, C., Goris, N., Gupta, A., He, Y. C.,
705 Olivie, D., Seland, O., and Schulz, M.: Ocean biogeochemistry in the Norwegian Earth System Model version 2
(NorESM2). *Geoscientific Model Development*, 13(5), 2393-2431. <https://doi.org/10.5194/gmd-13-2393-2020> ,
2020.
- Tokinaga, H., and Xie, S. P.: Weakening of the equatorial Atlantic cold tongue over the past six decades. *Nature Geoscience*,
4(4), 222-226. <https://doi.org/10.1038/Ngeo1078> , 2011.
- 710 Toniazzo, T., Bentsen, M., Craig, C., Eaton, B. E., Edwards, J., Goldhaber, S., Jablonowski, C., and Lauritzen, P. H.:
Enforcing conservation of axial angular momentum in the atmospheric general circulation model CAM6.
Geoscientific Model Development, 13(2), 685-705. <https://doi.org/10.5194/gmd-13-685-2020> , 2020.
- Toniazzo, T., and Koseki, S.: A Methodology for Anomaly Coupling in Climate Simulation. *Journal of Advances in
Modeling Earth Systems*, 10(8), 2061-2079. <https://doi.org/10.1029/2018ms001288> , 2018.
- 715 Vazquez, R., Parras-Berrocal, I., Cabos, W., Sein, D. V., Mananes, R., and Izquierdo, A.: Assessment of the Canary current
upwelling system in a regionally coupled climate model. *Climate Dynamics*, 58(1-2), 69-85.
<https://doi.org/10.1007/s00382-021-05890-x> , 2022.
- Vieira, L. H., Krisch, S., Hopwood, M. J., Beck, A. J., Scholten, J., Liebetrau, V., and Achterberg, E. P.: Unprecedented Fe
delivery from the Congo River margin to the South Atlantic Gyre. *Nature Communications*, 11(1).
720 <https://doi.org/ARTN/556>, 10.1038/s41467-019-14255-2 , 2020.
- Voldoire, A., Exarchou, E., Sanchez-Gomez, E., Demissie, T., Deppenmeier, A. L., Frauen, C., Goubanova, K., Hazeleger,
W., Keenlyside, N., Koseki, S., Prodhomme, C., Shonk, J., Toniazzo, T., and Traore, A. K.: Role of wind stress in
driving SST biases in the Tropical Atlantic. *Climate Dynamics*, 53(5-6), 3481-3504.
<https://doi.org/10.1007/s00382-019-04717-0> , 2019.
- 725 Xu, Z., Chang, P., Richter, I., Kim, W., and Tang, G. L.: Diagnosing southeast tropical Atlantic SST and ocean circulation
biases in the CMIP5 ensemble. *Climate Dynamics*, 43(11), 3123-3145. <https://doi.org/10.1007/s00382-014-2247-9> ,
2014.